Surface Science 98 (1980) 515-532
© North-Holland Publishing Company and Yamada Science Foundation

PLASMONS IN INVERSION LAYERS

Thomas N. THEIS

Thomas J. Watson Research Center, Yorktown Heights, New York 10598, USA *

Received 30 July 1979

The theoretical literature on plasmons in inversion layers is briefly reviewed. Predictions of the plasmon dispersion can be tested in experiments in which far infrared radiation is coupled to inversion layer plasmons by a grating structure forming the gate of an MOS device. A description of the far infrared transmission of such a device aids in interpreting the experimental results. The results to date generally show a remarkable agreement with simple theory, although interesting deviations are seen at low densities. Some recent work at plasmon wave numbers up to $q \simeq 0.14 \ k_{\rm F}$ is presented.

1. Introduction

Recent years have seen the development of a variety of far infrared (FIR) spectroscopic techniques for probing the inversion layer. Cyclotron resonance, first observed by Abstreiter et al. [1] and Allen et al. [2], measures the dynamical conductivity $\sigma_{xx}(\omega,B)$ parallel to the oxide—silicon interface. The study of intersubband transitions, initiated by Wheeler and Goldberg [3] and Kamgar et al. [4], probes the conductivity $\sigma_{zz}(\omega)$ perpendicular to the interface. Here we review the development of another spectroscopy, that of inversion layer plasmons [5–10].

As in cyclotron resonance experiments, an infrared radiation field probes the dynamical conductivity, $\sigma_{xx}(\omega)$. In this case, however, a spatially modulated field excites a different type of resonance, the plasma oscillation, or plasmon, in which the electric restoring forces created by inhomogeneities in the inversion layer charge density determine the resonant frequency.

A considerable body of theoretical work on the plasmon dispersion [11–27] aids in the interpretation of experiments. This work is reviewed in section 2, with special attention given to a simple model in which the inversion layer is considered to be an ideal two-dimensional (2D) electron gas. The results of this approach are compared to the results of more sophisticated models. In section 3, the use of a metallic grating structure to couple an FIR field to plasmons of specific wave number is discussed. Section 4 reviews the experimental work. The dependence of the

^{*} Part of this work has been carried out at the Physik-Department, Technische Universität München, D-8046 Garching, Fed. Rep. of Germany.

plasmon dispersion on inversion layer density [5,8], wave number [7,9], and magnetic field [6] has been investigated. Most of the results can be explained in terms of the classical long-wavelength conductivity for a 2D free electron gas, but interesting deviations from this simple picture are seen at low density [5,8] and in a magnetic field [6]. Finally, some recent results are presented which extend the wave number and frequency range of the previous work.

Although this review is limited to the special case of the inversion layer on (100) silicon, plasmons should be a useful tool for studying the dynamical conductivity in other space charge layer systems as well. Indeed, the observation of plasmons in the 2D system of electrons on the surface of liquid helium by Grimes et al. [28] preceded and stimulated the work on inversion layers. The recent observation of coupled ripplon—longitudinal plasmon modes, proving the existence of the Wigner lattice on liquid helium [29], is another outstanding contribution.

2. The plasmon dispersion relation

2.1. Simple theory

An approach taken by many authors in calculating the plasmon dispersion is to regard the inversion layer as a two-dimensional electron gas with conductivity tensor $\sigma(q, \omega)$. By this it is meant that a longitudinal electric field

$$E(q, \omega) = E(z) \exp(i\mathbf{q} \cdot \mathbf{r} - i\omega t)$$

produces a sheet current density at the inversion layer

$$j(\mathbf{q},\,\omega)\,\delta(z) = \sigma(\mathbf{q},\,\omega)\cdot \mathbf{E}(\mathbf{q},\,\omega)\,\delta(z)\;. \tag{2.1}$$

Here q and r are vectors in the x-y plane, and the inversion layer is assumed to be at z=0. Considering the total field to be the sum of external and induced fields,

$$E(q, \omega) = E^{\text{ex}}(q, \omega) + E^{\text{ind}}(q, \omega), \qquad (2.2)$$

an expression for E^{ind} in terms of E^{ex} is readily derived.

For clarity, consider a simple model where an oxide of thickness d and dielectric constant ϵ_{ox} separates the inversion layer from a metallic gate. The gate is assumed highly conducting and of unbounded thickness. Below the inversion layer is the silicon substrate (dielectric constant ϵ_s) which is also unbounded. We assume a longitudinal field acting in the x direction,

$$E_x^{\text{ex}}(q,\omega) = E_x^{\text{ex}} \exp(iq_x x - i\omega t)$$
.

Retardation effects associated with the finite speed of light are neglected, and Poisson's equation and the equation of continuity are solved together with eq. (2.1) to give the induced field at the inversion layer,

$$E_x^{\text{ind}}(q,\omega) = -E_x^{\text{ex}}(q,\omega) i \frac{q}{\omega} \frac{\sigma_{xx}(q,\omega)}{i(q/\omega) \sigma_{xx}(q,\omega) + \epsilon_s + \epsilon_{ox} \coth(qd)}.$$
 (2.3)

Since this field provides the restoring force for oscillations in the inversion layer charge density, the plasmon dispersion can be obtained simply by solving for resonances in eq. (2.3). Note that because the electric field extends into the media surrounding the inversion layer, the dispersion must depend on the geometry and properties of these media.

These results can be put in a more elegant form if eq. (2.2) is used to derive a constitutive relationship between E and $E^{\rm ex}$. Using a notation due to Ando [26] we may write

$$\sigma_{xx}(q,\omega) E_x(q,\omega) = \widetilde{\sigma}_{xx}(q,\omega) E_x^{ex}(q,\omega),$$
 (2.4a)

where

$$\tilde{\sigma}_{xx}(q,\,\omega) = \sigma_{xx}(q,\,\omega)\,\tilde{\epsilon}(q,\,\omega)^{-1}$$
, (2.4b)

with

$$\tilde{\epsilon}(q, \omega) = 1 + \frac{i}{\omega} \frac{q}{\epsilon_s + \epsilon_{ox} \coth(qd)} \sigma_{xx}(q, \omega)$$
 (2.4c)

The effect of the surrounding media is thus expressed in terms of an effective conductivity $\tilde{\sigma}_{xx}$ and effective dielectric constant $\tilde{\epsilon}$. The plasmon dispersion is obtained from the solution(s) of

$$\widetilde{\epsilon}(q,\,\omega) = 0$$
 (2.5)

The calculation can be carried further by assuming a specific form for σ_{xx} . For plasmon wavelengths large compared to the average interelectron spacing, we may use the Drude conductivity

$$\sigma_{xx} = \frac{n_s e^2 \tau}{m^*} \frac{1}{1 - i\omega \tau},\tag{2.6}$$

where n_s is the surface density of inversion layer electrons, m^* is the effective mass for motion parallel to the oxide—semiconductor interface, and τ is a phenomenological relaxation time. Substituting eq. (2.6) into eq. (2.5) and taking the limit $\tau \to \infty$, we obtain

$$\omega^2 = \frac{n_s e^2}{m^*} \frac{q}{\epsilon_s + \epsilon_{ox} \coth(qd)}.$$
 (2.7)

We now identify ω and q as the plasmon frequency and wave number, respectively. This dispersion has been obtained by several authors including Chaplik [12] and Nakayama [14]. Experiments which have verified this relationship for inversion layer plasmons are discussed in section 4.

If
$$qd \gg 1$$
, eq. (2.7) reduces to

$$\omega_0^2 = \frac{n_s e^2 q}{2m^* \overline{\epsilon}},\tag{2.8}$$

where $\overline{\epsilon} = \frac{1}{2}(\epsilon_s + \epsilon_{ox})$. The square root dependence of the plasmon energy on wave number is a result first given for 2D systems by Ritchie [30] and Ferrel [31]. If $qd \leq 1$, then at fixed q, it can be shown that bringing the gate closer to the inversion layer (decreasing d) always decreases ω . This reflects the reduction in the restoring forces for charge density oscillations in the inversion layer, as E^{ind} is partially screened by image charges in the gate [12].

2.2. Retardation effects

For values of ω , q, n_s , and d corresponding to the experiments described in section 4, it is easy to show that eq. (2.7) always satisfies the condition $q \gg k_L$, where $k_L = \omega/c$ is the light wave number. This suggests that neglect of retardation in the derivation of eqs. (2.3) through (2.7) was justified. This is confirmed by comparison with the results of Eguiluz et al. [17] who solved Maxwell's equations for the same system. The results are experimentally indistinguishable from eq. (2.7). However, in the absence of a screening gate to reduce the range of $E^{\rm ind}$, retardation effects can be important and have been considered by many authors [11,13–17, 22,25]. In particular, Stern [11] showed that as $q \to 0$, the dispersion approaches, but does not cross the light line. The plasmon mode is thus non-radiative for this simple geometry.

2.3. Other geometries

Interesting variations from eq. (2.7) will arise if the geometry and properties of the surrounding media are varied. Eguiluz et al. [17] considered the coupling that arises between gate and inversion layer plasmon modes for the three cases where the gate is composed of a metal, a semimetal, or another semiconductor. Caille et al. [22] studied the case of a gate of finite thickness. Here the gate has two plasmon modes, one of which is quasi-longitudinal and the other quasi-transverse, both of which can be coupled to the inversion layer plasmon. In general, significant coupling of gate and inversion layer modes occurs only at frequencies and wave numbers where the uncoupled modes would cross. For the case of a metallic gate, the crossing is at frequencies and wave numbers too high to be accessible. The semimetal and semiconductor cases may be more accessible to experimental investigation.

Recently, Chaplik and Krasheninnikov [27] investigated the coupling between inversion layer plasmons and the piezo-acoustic modes of a piezoelectric crystal. An interesting result is that under certain conditions, damping of the plasmon occurs by radiation of sound into the bulk piezocrystal. It will be interesting to see if technical applications can be found for this system.

2.4. Dispersion in the conductivity, finite inversion layer thickness

As the plasmon wavelength approaches the mean interelectron spacing, the q dependence (dispersion) in the conductivity will alter the behavior of the plasmon

dispersion. Using the random phase approximation, Stern [11] obtained

$$\omega^2 \simeq \omega_0^2 \left(1 + \frac{1}{g_V} \frac{3}{4} a_0 q \right), \tag{2.9}$$

where $a_0 = 4\pi \overline{e}\hbar^2/m^*e^2$ is the effective Bohr radius for an inversion layer electron, g_v is the valley degeneracy, and ω_0 is given by eq. (2.8). A hydrodynamic calculation by Fetter [13] shows that the second term may be considered to arise from the finite compressibility of the 2D electron gas.

Beck and Kumar [23] showed that inclusion of correlation effects produces an additional term of opposite sign and of the same order of magnitude as the second term in eq. (2.9). Rajagopal [24] pointed out a correction to their result, and gave an expression which can be written as

$$\omega^2 \simeq \omega_0^2 \left(1 + \frac{1}{g_V} \frac{3}{4} a_0 q - \frac{1}{g_V} \frac{5}{6\pi} \frac{q}{k_F} \right). \tag{2.10}$$

Jonson [20] investigated the plasmon dispersion using three different approximations to the many body problem, and found that the results were very model dependent, especially at low densities where correlation effects are important. Observation of the plasmon dispersion for $q \sim k_{\rm F}$ may thus test the ranges of validity of various many body theories. This is a very interesting area open to investigation.

At plasmon wavelengths short enough for many body effects to be important, the finite thickness of the inversion layer must also be considered. Jonson [20] found significant changes in the plasmon dispersion although the general trend predicted by each many body theory was unaffected. Beck and Kumar [23] gave a simple correction to the dispersion of the same magnitude as the many body effects. Using realistic wave functions to describe the extension of the inversion layer perpendicular to the oxide—semiconductor interface, Dahl and Sham [25] made an extensive study of the electrodynamics of the inversion layer in the random phase approximation. In a unified treatment they obtained both the intersubband transitions and plasmons as, respectively, the transverse and longitudinal electromagnetic modes of the system. Some analogous results had previously been suggested by Chen et al. [32], who considered the electromagnetic modes of a charged slab model of the inversion layer.

2.5. Magnetoplasmon dispersion

The plasmon dispersion in the presence of a magnetic induction, B, perpendicular to the inversion layer is easily obtained in the long-wavelength limit. For a 2D free electron gas we have

$$\sigma_{xx} = \frac{1}{2}(\sigma_+ + \sigma_-) \,, \tag{2.11a}$$

where

$$\sigma_{\pm} = \frac{n_{\rm s}e^2\tau}{m^*} \frac{1}{1 - \mathrm{i}(\omega \pm \omega_{\rm c})\tau},\tag{2.11b}$$

and $\omega_c = eB/m^*$ is the cyclotron resonance frequency. Substituting σ_{xx} into eq. (2.5) and again letting $\tau \to \infty$, we find

$$\omega^2 = \omega_p^2 + \omega_c^2 \,, \tag{2.12}$$

where ω_p is the B=0 plasmon frequency given by eq. (2.7). This result has been pointed out by Horing and Yildiz [21], and can be derived in the proper limits from the results of other authors [12,15,16,19].

Eqs. (2.11) do not describe some important characteristics of the observed long-wavelength dynamical conductivity. In particular, the presence of poles at $\omega \simeq \nu \omega_c$ where $\nu=2,3,...$ corresponds to the subharmonic structure observed by Abstreiter et al. [1], and explained by Ando [33,34]. In Ando's theory, this structure arises through the action of short range scattering centers; the strength of the poles vanishes as $\tau \to \infty$. It is therefore not possible to speak of changes in the dispersion given by eq. (2.12) in this limit. Nevertheless, the presence of these poles in the conductivity can cause strong changes in the observed magnetoplasmon resonance line shape [26]. The observation of such effects is discussed fully in section 4.

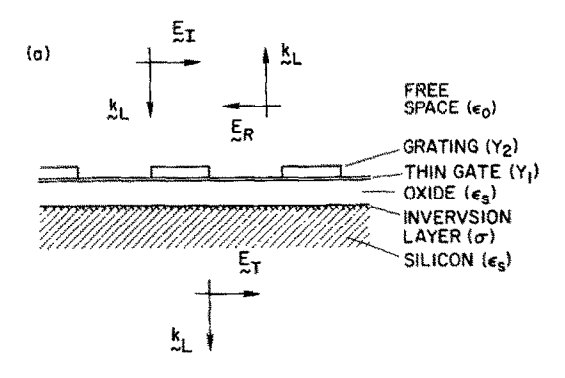
Interestingly, a consideration of dispersive effects in the magnetoconductivity also leads to poles at $\omega \simeq \nu \omega_c$ where $\nu = 2, 3, ...$ [35]. These give rise to additional branches in the magnetoplasmon dispersion given also by $\omega \simeq \nu \omega_c$, as well as slightly altering eq. (2.12). Precise results have been given by Chiu and Quinn [15] and Horing and Yildiz [21] using the random phase approximation and by Lee and Quinn using the Fermi Liquid Model [16]. For the present experimentally obtained values of q, the effect of these modes on the magnetoplasmon lineshape is overwhelmed by the effect of the subharmonic mode [26]. The dispersive effects should, however, be observable at larger wave numbers.

3. Coupling to a far infrared field

3.1. General considerations

As discussed in the previous section, the plasmon modes are non-radiative. They can, however, be coupled to a probing electromagnetic field by a metallic grating. Fig. 1a illustrates the geometry of a typical experimental MOS device. As in cyclotron resonance experiments [1,2], a thin high resistivity gate allows transmission of far infrared (FIR) radiation. Here, however, the adjoining grating of highly conductive metal spatially modulates the FIR field in its vicinity, making possible the excitation of plasmon resonances.

Momentum exchange with a perpendicularly indicent plane wave allows coupling



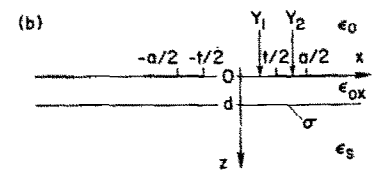


Fig. 1. (a) MOS device with grating on the gate. (b) Model for calculating the far infrared transmission.

to plasmons when

$$q_n = n \ 2\pi/a \ , \qquad n = 1, 2, \dots,$$
 (3.1)

where a is the grating periodicity. How will this coupling affect the transmission? Using the simple model of the plasmon dispersion outlined in the previous section, the space and time averaged absorption of power from an external longitudinal field by the inversion layer is

$$\overline{p} = \frac{1}{2} |E_x^{\text{ex}}(q, \omega)|^2 \text{ Re } \widetilde{\sigma}_{xx}(q, \omega) , \qquad (3.2)$$

where $\tilde{\sigma}_{xx}$ is given by eq. (2.4b). From eqs. (2.4a) and (2.4b) it can be seen that a zero in $\tilde{\epsilon}(q,\omega)$ generally corresponds to a pole in \bar{p} , so a plasmon resonance absorbs power from the field. If the absorption is small, the change in transmission will be proportional to \bar{p} .

3.2. Calculation of the FIR transmission

Experimentally it is convenient to measure the relative change in transmission, $P = -\Delta T/T$, caused by the presence of the inversion layer. An expression for P has been given by Allen et al. [5], and the approximations leading to this result have been discussed elsewhere [8]. Here we consider an algebraically equivalent result

[6] based on the use of eq. (3.2). The purpose is to give a physically intuitive picture of the grating mediated coupling between the FIR field and the plasmon resonance.

As shown in fig. 1b, the grating/gate (hereafter referred to as simply the grating) is modeled as a vanishingly thin layer consisting of alternating strips of low and high conductivity, Y_1 and Y_2 . The strips are of widths t and a-t respectively. For FIR wavelengths, $\lambda \gg a$, Poisson's equation may be solved for the near field under the boundary conditions imposed by the grating and the presence of the far fields. Calculating the near field in the low frequency limit where, to a good approximation, the grating current is spatially constant [36], one obtains

$$P \cdot \frac{1}{2} (Y_0 + Y_s + Y_g) = \text{Re } \sigma_{xx} (q = 0, \omega)$$

$$+ \sum_{n=1}^{\infty} \left[\frac{2 \sin^2(q_n t/2)}{(q_n t/2)^2} \right] \left[\frac{Y_2 - Y_1}{Y_2 + Y_1 (a/t - 1)} \right]^2 \left[\frac{\coth^2(q_n d) - 1}{[\epsilon_s / \epsilon_{ox} + \coth(q_n d)]^2]} \right]$$

$$\times \text{Re } \widetilde{\sigma}_{xx} (q_n, \omega)$$
(3.3)

Here, Y_0 and Y_s are the admittances of the free space and silicon respectively, and Y_g is the grating admittance in the limit $\omega \to 0$. The factor labeled "1" arises from the average strength squared of the *n*th Fourier component of the longitudinal field at the grating, the factor labeled "2" arises from the decrease in strength of the component at distances d from the grating, and Re $\tilde{\sigma}_{xx}(q_n,\omega)$ describes the plasmon lineshape. Note again that resonances in P are directly related to the plasmon dispersion through eqs. (2.4b) and (2.5).

3.3. Sample design

Besides providing a good account of the experimental results discussed in section 4, eq. (3.3) contains the information needed to design samples which provide optimum coupling between plasmon resonances and the FIR field. Under the experimental conditions of interest, $Y_2 \gg Y_1$. The factor labeled "1" is then proportional to $\sin^2(q_nt/2)/(q_nt/2)^2$. In order to maximize this term at a given grating periodicity, a, the open space, t should be made as small as possible. This is especially true for n > 1. Qualitatively this may be understood as arising from the concentration of the longitudinal electric field across the open space of the grating. Reducing the size of the opening, i.e., making the ratio t/a smaller, increases the relative strength of the higher spatial Fourier components of the field. Plasmons of large q_n may be excited.

The term labeled "2" in eq. (3.3) arises from the exponential decay of the spatially modulated part of the electric field away from the grating, modified by the dielectric image effects. This is easily seen for the special case $\epsilon_s = \epsilon_{ox}$, when the term reduces to $\exp(-2q_n d)$. Strong coupling is thus obtained only when $d/a \le 1$.

Note that the conditions $t/a \le 1$, $d/a \le 1$ must also be satisfied by efficient plas-

mon emission devices. In these devices, discussed by Gornik [10], emission is through radiative decay of plasma oscillations coupled to the external field by the grating.

There are technical limits on how thin the oxide can be made, but a technique called shadowing substantially reduces the problems in making gratings with small t/a. (See Jelks et al. [46] and references therein for a discussion of similar techniques.) As discussed by Theis et al. [7,9] a grating is first fashioned from metal using standard lithographic techniques. Highly conductive metal is then evaporated onto the structure from an angle such that all but a small part of the grating gap (the shadowed area) is covered. In section 4, gratings fashioned by electron beam lithography are described. With the aid of shadowing, these have allowed observation of plasmon resonances with wavelengths as small as $0.2 \mu m$, corresponding to q_5 .

4. Observation of inversion layer plasmons

4.1. Experimental notes

Typical inversion layer scattering times are on the order of 10^{-12} s. Observation of a well-defined plasmon resonance requires $\omega \tau > 1$; hence the need for frequencies in the far infrared. As FIR sources, transmission experiments have utilized the Fourier spectrometer [5] and molecular gas lasers [6,9]. The Fourier transform technique, discussed by Tsui et al. [8], allows ω to be swept while other variables are held constant. The laser experiments are conducted at fixed ω , the resonance being swept by varying n_s or B.

The samples are MOS transistors [5] or capacitors [6,9] with grating structures as discussed in the previous section. Oxide thickness, d, is typically $\sim 0.1 \, \mu m$ and values of the grating periodicity, a, have ranged between 1.0 and 5.0 μm . Gate areas are $\sim 5 \, \text{mm}^2$. FIR radiation is focused through the gate by a condensing cone, and passes on to a detector. By square wave modulating the gate voltage during the measurement, a difference signal proportional to the change in transmission caused by the presence of the inversion layer is obtained.

When MOS capacitors are used, $V_{\rm g}$ is applied between the gate and a back contact. Since at low temperatures the silicon substrate is highly insulating, sufficient minority carriers for charging the inversion layer must be supplied by band gap radiation from a light-emitting diode. Varying the intensity of this radiation shifts the conduction threshold voltage. Measured as a function of gate voltage, the plasmon resonance also shifts, paralleling the change in threshold voltage [37]. The inversion layer carrier density at resonance remains unchanged. Thus, no change in the plasmon dispersion is observed as a function of band gap radiation over a wide range of illumination intensities. Apparently, the steady state density of free carriers induced in the bulk silicon is too low to significantly screen the plasmon

electric field. The assumption of an insulating silicon substrate used to derive eqs. (2.3) through (2.5) is therefore justified. At high temperatures in heavily doped substrates, screening by the bulk silicon carriers might become important.

4.2. Density dependence

The first experimental investigation of inversion layer plasmons was made by Allen et al. [5]. Plasmon resonances were obtained for a value of $q = 2\pi/a$ with $a = 3.5 \,\mu\text{m}$. An expression equivalent to eq. (3.2) was used to fit the observed transmission spectrum. For $n_{\rm s} > 10^{12} \, \text{cm}^{-2}$, remarkable agreement was found with this expression using the Drude conductivity, eq. (2.6), with $m^* = 0.2 m_0$ and τ determined from the dc conductivity. This is a confirmation of both the dispersion given by eq. (2.7) and the Drude relaxation at high frequencies.

At lower densities significant deviations from the predicted resonant frequencies were observed. It was pointed out that the deviations could be accounted for in terms of the Drude conductivity by assuming a lower value of n_s or a larger value of m^* . Anomalously large values of m^* have been measurd in cyclotron resonance at low densities, so the plasmon data were also interpreted in this manner. The values of m^* obtained from the plasmon energies were found to be significantly larger than cyclotron resonance values measured on the same sample [8]. This effect deserves further study since it may shed light on the nature of the localization mechanism at low densities.

4.3. Wave number dependence

By employing shadowed gratings with small values of t/a, Theis et al. [9] were able to observe plasmon resonances with $q_n = n2\pi/a$ where n = 1, 2, and 3. With $d = 0.22 \,\mu\text{m}$ and $a = 5 \,\mu\text{m}$, the gate screening was strong for n = 1 but relatively weak for n = 3, providing a stringent test of the q dependence given by eq. (2.7).

Fig. 2 shows data obtained at FIR wavelengths of 311 and 195 μ m. P is recorded as a function of n_s . The data clearly shows peaks corresponding to the resonant values of n_s (inverted triangles) as calculated from eq. (2.7) with $q = q_n$. The resonances are superposed on a monotonically increasing Drude background, corresponding to absorption of power from the spatially unmodulated (n = 0) component of the radiation field by the inversion layer.

The dotted lines give fits to the lineshape predicted by eq. (3.3) with independently measured values of t, a, and d. The n_s dependences of m^* and τ were determined from cyclotron resonance measurements at $\lambda = 337~\mu m$ after the grating was chemically stripped from the gate. Because τ depends on magnetic field [33,34], the cyclotron resonance values are scaled by an n_s independent factor of 1.2 to give a better fit to the plasmon resonance width. The plasmon resonance thus measures a larger scattering time than the cyclotron resonance, in qualitative agreement with theory and with the measurements of Abstreiter et al. [38] who compared τ at

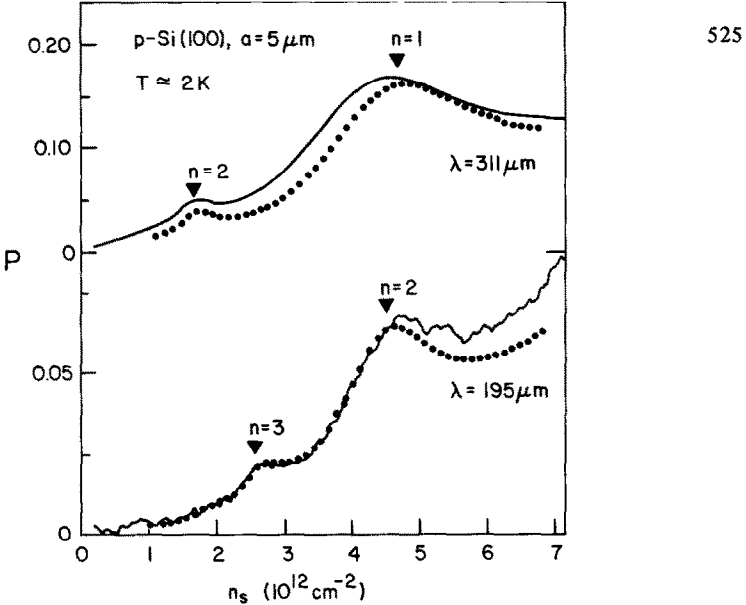


Fig. 2. Relative change in transmission, P, versus electron density, n_s , at 311 and 195 μm far infrared wavelengths. Inverted triangles give plasmon resonance positions predicted by eq. (2.7). Dotted lines are theory based on eq. (3.3). (From ref. [9].)

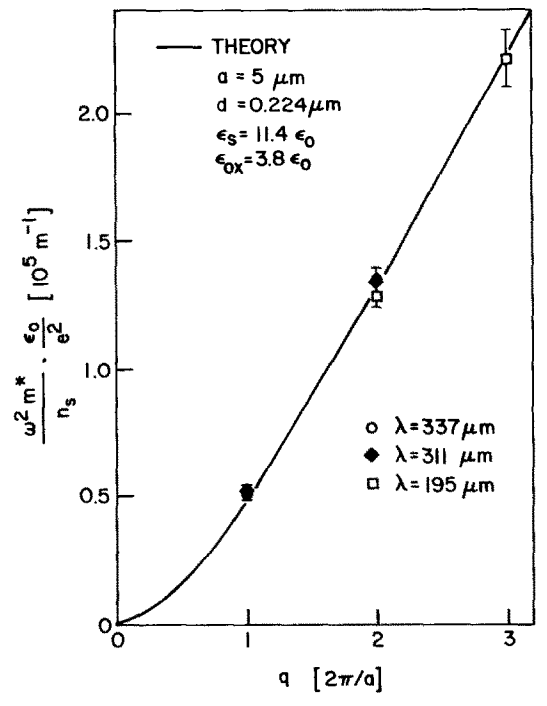


Fig. 3. Resonant values of $\omega^2 m^*/n_s$ as a function of wave number, q. ω^2 is determined from the laser frequency, m^* from cyclotron resonance measurements, and n_s from data such as that of fig. 2. (From ref. [9].)

cyclotron resonance with τ obtained from low frequency B = 0 measurements.

Fig. 3 shows the resonant values of $\omega^2 m^*/n_s$ as a function of q. The resonant values of n_s are taken from data including those of fig. 2. The theoretical line is determined from eq. (2.7), and the agreement with experiment is generally very good.

4.4. Magnetoplasmons

The magnetoplasmon dispersion, eq. (2.12) obtained for the classical long-wavelength conductivity may be rewritten for the resonant value of the magnetic induction. If m^* is approximately constant as a function of n_s , one obtains

$$B \simeq B_c (1 - n_s/n_{s0})^{1/2}$$
, (4.1)

where $B_c = m^* \omega / e$, the cyclotron resonant value of B, and n_{s0} is the plasmon resonant value of n_s when B = 0.

The predictions of this equation are found to be in general agreement with the results of an experiment by Theis et al. [6]. Fig. 4 shows the magnetoplasmon behavior as a function of B at an FIR wavelength of 337 μ m. With $t/a \approx 0.5$, only the magnetoplasmon resonance excited by the n=1 Fourier component of the electric field is important. Resonances for $n \geq 2$ are too small to be observed. As predicted by eq. (4.1), for low values of n_s , as in curve h, $B \approx B_c$. The normal cyclotron resonance peak (corresponding to the n=0 component of the field) is seen, with an additional contribution from the magnetoplasmon resonance. At higher n_s , the magnetoplasmon moves to lower values of B, as can be seen in curves g through g. It first appears as a distortion of the cyclotron resonance lineshape, and then separates from it entirely to form a distinct peak. For $n_s > n_{s0}$ (curves g and g only the tail of the resonance is evident.

The theory (dashed line) based on the classical long-wavelength conductivity cannot explain the splitting of the magnetoplasmon peak at $B \simeq \frac{1}{2}B_c$ in curves e and f. Samples with stronger coupling to the plasmon resonance $(t/a \simeq 0.15)$ show an additional splitting at $B \simeq \frac{1}{3}B_c$ [37]. This splitting of the magnetoplasmon peak as it crosses $B \simeq B_c/\nu$, $\nu = 2, 3, ...$ can be associated quite generally with the occurrence of poles in the conductivity at $\omega \simeq \nu \omega_c$. (Here we refer implicitly to the real part of the complex resonant frequency.) In fact, such poles are observed as cyclotron subharmonic resonances [38], and can be shown in a quantum mechanical calculation to arise from transitions between non-adjacent Landau levels [33,34].

Fig. 5 gives results of a calculation by Ando [26] showing how the splitting arises. The solid lines are generated using the expression for σ_{xx} given in ref. [26], while the dotted lines are obtained from the classical conductivity. The signal is proportional, in Ando's notation, to Re σ_{eff} = Re σ_{xx} + δ_1 Re $\tilde{\sigma}_{xx}$, where Re σ_{xx} and Re $\tilde{\sigma}_{xx}$ correspond to the CR and magnetoplasmon absorption respectively. The scale factor δ_1 = 0.23 is appropriate for the sample parameters corresponding to fig. 4.

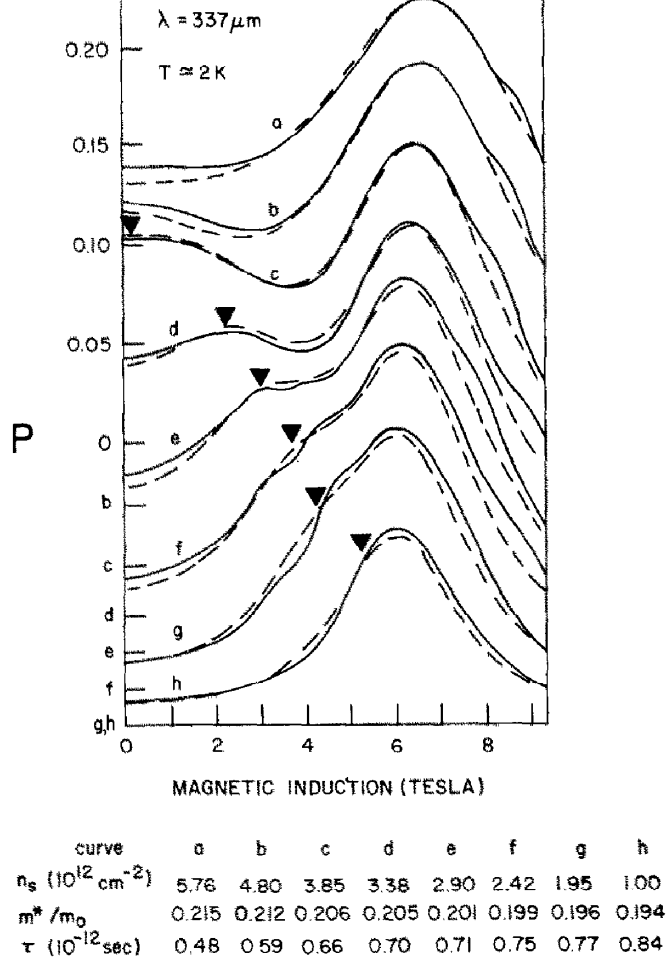


Fig. 4. Relative change in transmission, P, versus magnetic induction, B, for fixed values of electron density, n_s , as listed above. Inverted triangles represent the magnetoplasmon resonance position calculated from eq. (2.12). (From ref. [6].)

The structure in Re σ_{xx} around 34 kOe, denoted by the upward pointing arrow, is the subharmonic resonance. The magnetoplasmon peak (downward pointing arrow) is split due to its presence. Although the peak in Re σ_{xx} partially fills in the trough in Re σ_{xx} , the net result in Re σ_{eff} is a splitting, much like that which is observed. The splitting is observable only when $\omega \simeq 2\omega_c$, since only then do the subharmonic and magnetoplasmon modes interact and repel each other.

It is emphasized that the effect is general. Any theory which gives a good

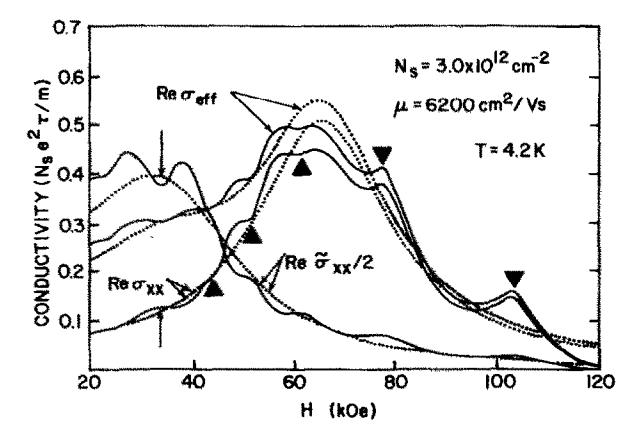


Fig. 5. Magnetoplasmon lineshape calculated by Ando (from ref. [26]). Re σ_{xx} and Re $\tilde{\sigma}_{xx}$ describe the cyclotron and magnetoplasmon resonances, respectively. The change in transmission is proportional to Re $\sigma_{\rm eff}$. The positions of the subharmonic structure and the classically predicted magnetoplasmon resonance are denoted by upward and downward pointing arrows respectively.

account of the strength of the observed subharmonic resonance, will also predict the observed splitting.

4.5. Recent results

Recently electron beam lithography [39] has been employed to extend the wave number and frequency range of the plasmon observations. The samples were fabricated on $0.2~\Omega$ cm (100) silicon and had a gate oxide with $d=0.054~\mu{\rm m}$ upon which a chrome gate electrode of roughly $0.07~\mu{\rm m}$ thickness had been evaporated. The grating pattern was written by the electron beam in $0.4~\mu{\rm m}$ thick PMMA resist which had been spun cast on the gate. The resist image formed a mask for chemical wet etching of the chrome. The resulting grating, with $a=1.0~\mu{\rm m}$ and $t/a\sim0.5$, was then coated with a thin NiCr film and finally shadowed, reducing t/a to ~0.1 .

Fig. 6 shows results obtained at several laser frequencies. The derivative of P with respect to gate voltage, $V_{\rm g}$, was measured as a function of inversion layer density. This emphasizes the plasmon resonance with respect to the slowly varying Drude background. The dotted lines are calculated from eq. (3.3), with $m^* = 0.2m_0$ and assuming $\tau = 4.5 \times 10^{-13}$ s for fig. 6a and $\tau = 3.75 \times 10^{-13}$ s for fig. 6b. These scattering times show the mobility is low with a broad, not well defined peak, consistent with some damage to the oxide during the electron beam fabrication of the grating.

A few words regarding the data analysis are appropriate. The measured values of d and a are believed accurate to within 2%. ϵ_s is known from FIR measurements at

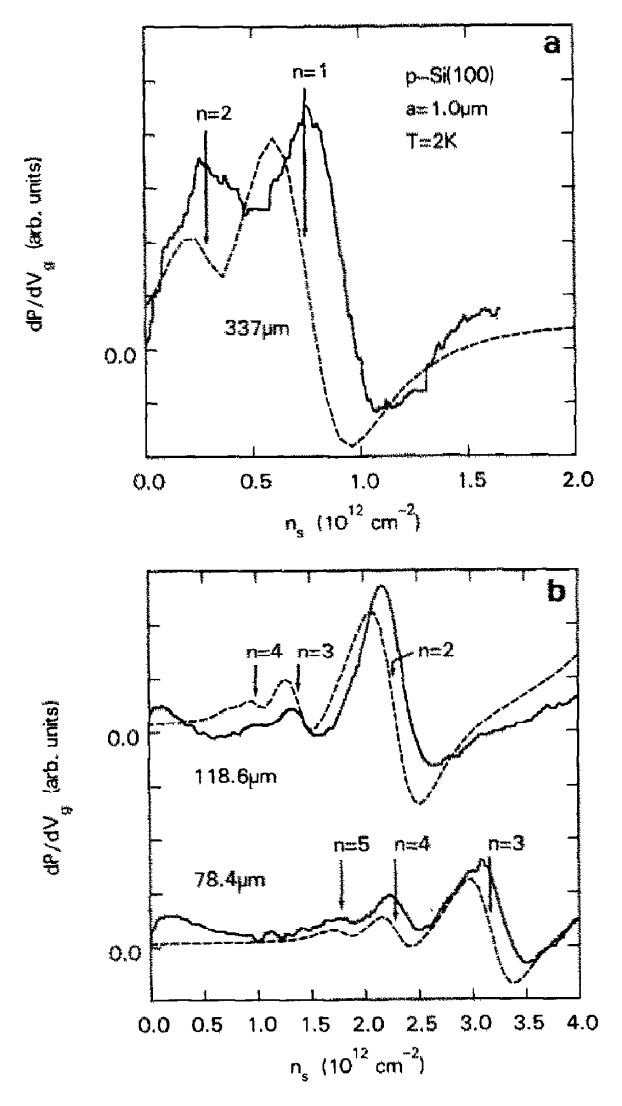


Fig. 6. The derivative of the relative change in transmission with respect to gate voltage, dP/dV_g . Theory from eq. (3.3) is given by dashed lines, data by solid lines; (a) 337 μ m infrared wavelengths; (b) 78.4 and 118.6 μ m infrared wavelengths.

T=2 K [41]. For the frequency range of interest here it may be taken to be $\epsilon_{\rm s}=11.45$ with negligible error. FIR measurements of $\epsilon_{\rm ox}$ are not available, but measurements made at optical frequencies [42] suggest that values for fused quartz are appropriate. The measured values for fused quartz at room temperature [43]

were therefore assumed, giving $\epsilon_{ox} = 3.81$ at the lowest frequency used and rising by two percent at the highest frequency.

The threshold gate voltage for conduction at high frequency was observed and used together with measurements of quantum oscillations in the magnetoconductivity to determine $n_{\rm s}$ as a function of gate voltage. These measurements are believed generally accurate to within three percent. In this case, however the samples have been irradiated by an electron beam, which is known to introduce interface states in the band gap [44]. Fowler and Hartstein [45] have shown that such states result in a nitrogen temperature threshold voltage shifted to lower values than the voltage determined by magnetoconductance oscillations. If the high frequency onset of conductivity also displays such a shift, a systematic error is introduced in determining $n_{\rm s}$.

For $n_{\rm s}>10^{12}~{\rm cm}^{-2}$ (fig. 6b) the agreement between theory and experiment is good. The deviations from the predicted resonant positions in $n_{\rm s}$ would imply an effective mass between three and five percent larger than the value assumed. This may indicate a systematic error in determining $n_{\rm s}$ as discussed above. The deviations in line *shape* can be mostly attributed to the fact that τ is not constant as a function of $n_{\rm s}$.

For $n_{\rm s} \lesssim 10^{12}~{\rm cm}^{-2}$ (fig. 6a) the deviation from the predicted resonant position is somewhat larger than the possible systematic error and must be interpreted as an increase in effective mass in the localization regime. This is qualitatively consistent with the trend observed by Allen et al. [5] and with cyclotron resonance measurements in the localization regime [40].

Note that the n=4 resonance observed at an infrared wavelength of 118 μ m corresponds to $q/k_F=0.14$. No significant shift of the resonance position attributable to a variation of the q dependence from that of eq. (2.7) is observed. This is consistent with eq. (2.10) which predicts less than a two percent change in the resonant value of n_s attributable to dispersive effects in the conductivity. The experiment does suggest the technical feasibility of observing plasmons with wavelengths not too much larger than the interelectron spacing. An accurate interpretation of such experiments will, however, require an understanding of the deviations from theory evident in fig. 6.

5. Conclusion

On (100) silicon, for n_s in the metallic conductivity regime, the validity of the simple theory of inversion layer plasmons based on the long wavelength conductivity σ_{xx} ($q=0,\omega$) has been demonstrated over a wide frequency and wave number range. The plasmon resonance can therefore be used as a tool to probe the conductivity in systems less well understood. The principal components of the dynamical conductivity tensor can be separately measured by changing the grating orientation, and m^* and τ can be determined in the absence of a magnetic field. The vari-

ous cyclotron resonance experiments [40] which have been so productive in recent years, will be complemented.

The extension of observations to $q \sim k_{\rm f}$, offers the possibility of obtaining novel results since the Fermi energy and wave number can be easily varied with respect to the plasmon energy and wave number. We may expect to see much more work on inversion layer plasmons in the next few years.

Acknowledgement

It is a pleasure to acknowledge many helpful discussions with J.P. Kotthaus, P.J. Stiles, T. Ando, B. Vinter and S.J. Allen. The author is indebted to J.F. Koch for hospitality at the Physik Department E-16 of the Technische Universität München, where much of the experimental work on inversion layer plasmons was done, and to J.P. Kotthaus, whose close collaboration and support helped make the work possible. Financial support for this work was provided by the Deutsche Forschungsgemeinschaft via SFB 128. The work on samples fabricated with electron beam lithography was done in collaboration with W.D. Grobman of the IBM T.J. Watson Research Center.

References

- [1] G. Abstreiter, P. Kneschaurek, J.P. Kotthaus and J.F. Koch, Phys. Rev. Letters 32 (1974)
- [2] S.J. Allen, D.C. Tsui and J.V. Dalton, Phys. Rev. Letters 32 (1974) 107.
- [3] R.G. Wheeler and H.S. Goldberg, IEEE Trans. Electron Devices ED-22 (1975) 1001.
- [4] A. Kamgar, P. Kneschaurek, W. Beinvogel and J.F. Koch, in: Proc. Intern. Conf. on the Physics of Semiconductors, Ed. M.H. Pilkuhn (Teubner, Stuttgart) p. 709.
- [5] S.J. Allen, Jr., D.C. Tsui and R.A. Logan, Phys. Rev. Letters 38 (1977) 980.
- [6] T.N. Theis, J.P. Kotthaus and P.J. Stiles, Solid State Commun. 24 (1977) 273.
- [7] T.N. Theis, J.P. Kotthaus and P.J. Stiles, Surface Sci. 73 (1978) 434.
- [8] D.C. Tsui, S.J. Allen, Jr., R.A. Logan, A. Kamgar and S.N. Coppersmith, Surface Sci. 73 (1978) 419.
- [9] T.N. Theis, J.P. Kotthaus and P.J. Stiles, Solid State Commun. 26 (1978) 603.
- [10] E. Gornik, R. Schwarz, G. Lindemann and D.C. Tsui, Surface Sci. 98 (1980) 493.
- [11] F. Stern, Phys. Rev. Letters 18 (1967) 546.
- [12] A.V. Chaplik, Zh. Eksperim. i Teor. Fiz. 62 (1972) 746 [Soviet Phys.-JETP 35 (1972) 395].
- [13] A.L. Fetter, Ann. Phys. (NY) 81 (1973) 367; Phys. Rev. B10 (1974) 3739.
- [14] M. Nakayama, J. Phys. Soc. Japan 36 (1974) 393.
- [15] K.W. Chiu and J.J. Quinn, Phys. Rev. B9 (1974) 4724.
- [16] T.K. Lee and J.J. Quinn, Phys. Rev. B11 (1975) 2144.
- [17] A. Eguiluz, T.K. Lee, J.J. Quinn and K.W. Chiu, Phys. Rev. B11 (1975) 4989.
- [18] G. Meissner, H. Namaizawa and M. Voss, Phys. Rev. B13 (1976) 1370.
- [19] G. Meissner, Z. Physik B23 (1976) 173.
- [20] M. Jonson, J. Phys. C9 (1976) 3055.

- [21] N.J.M. Horing and M.M. Yildiz, Ann. Physik 97 (1976) 216.
- [22] A. Caille and M. Banville, Solid State Commun. 19 (1976) 951.
- [23] D.E. Beck and P. Kumar, Phys. Rev. B13 (1976) 2859.
- [24] A.K. Rajagopal, Phys. Rev. B15 (1977) 4264.
- [25] D.A. Dahl and L.J. Sham, Phys. Rev. B16 (1977) 651.
- [26] T. Ando, Solid State Commun. 27 (1978) 895.
- [27] A.V. Chaplik and M.V. Krasheninnikov, Solid State Commun. 27 (1978) 1297. See also, A.V. Chaplik and M.V. Krasheninnikov, Surface Sci. 98 (1980) 533.
- [28] C.C. Grimes and G. Adams, Phys. Rev. Letters 36 (1976) 145.
- [29] C.C. Grimes and G. Adams, Phys. Rev. Letters 42 (1979) 795. See also, C.C. Grimes and G. Adams, Surface Sci. 98 (1980) 1.
- [30] R.H. Ritchie, Phys. Rev. 106 (1957) 874.
- [31] R.A. Ferrel, Phys. Rev. 111 (1958) 1214.
- [32] W.P. Chen, Y.J. Chen and E. Burstein, Surface Sci. 58 (1976) 263.
- [33] T. Ando, J. Phys. Soc. Japan 38 (1975) 989.
- [34] T. Ando, Phys. Rev. Letters 36 (1976) 1383.
- [35] M.H. Cohen, M.J. Harrison and W.A. Harrison, Phys. Rev. 117 (1960) 937.
- [36] This is equivalent to the condition discussed in ref. [8] that the capacitive part of the grating admittance is small compared to the resistive part.
- [37] T.N. Theis, unpublished data.
- [38] G. Abstreiter, J.P. Kotthaus, J.F. Koch and G. Dorda, Phys. Rev. B14 (1976) 2480.
- [39] T.H.P. Chang, A.D. Wilson, A.J. Speth and C.H. Ting, in: Proc. Intern. Conf. on Electron and Ion Beam Technology (The Electrochemical Society, Inc., 1976) p. 392.
- [40] For a review, see J.P. Kotthaus, Surface Sci. 73 (1978) 472.
- [41] E.V. Loewenstein, D.R. Smith and R.L. Morgan, Appl. Opt. 12 (1973) 398.
- [42] E.A. Taft, J. Electrochem. Soc. 125 (1978) 968.
- [43] T.J. Parker, J.E. Ford and W.G. Chambers, Infrared Phys. 18 (1978) 215.
- [44] E.H. Snow, A.S. Grove and D.J. Fitzgerald, Proc. IEEE 55 (1967) 1168.
- [45] A.B. Fowler and A. Hartstein, Surface Sci. 98 (1980) 169.
- [46] E.C. Jelks, G.L. Kerber and H.A. Wilcox, Appl. Phys. Letters 34 (1979) 28.